Theor Appl Climatol
DOI 10.1007/s00704-014-1215-y

ORIGINAL PAPER

Multidecadal variations in the modulation of Alaska wintertime air temperature by the Madden–Julian Oscillation

Eric C. J. Oliver

Received: 6 March 2014 / Accepted: 25 June 2014

Abstract The Madden–Julian Oscillation (MJO), the dominant mode of intraseasonal variability in the tropics, is known to influence extratropical air temperature in the Northern Hemisphere. In particular, it has been shown that intraseasonal variations in wintertime Alaska surface air temperature (SAT) is linked with variations in cross-shore surface wind and that this mechanism is driven by a train of Rossby waves originating in the tropics due to MJO forcing. We show, using long station records of Alaska SAT and an independent reconstruction of the MJO index over the twentieth century, that the MJO–SAT connection in Alaska has undergone significant multidecadal variability over the last century. The Pacific Decadal Oscillation appears to explain some of the observed multidecadal variability but fails to capture a large proportion of it. We identify four distinct periods between the years 1910 and 2000 that exhibit either a weak, moderate or strong MJO–SAT connection. The nature of our method ensures that the detected multidecadal variability is due to changes in the teleconnection mechanism and not due to changes in the strength of the MJO index. Finally, we speculate on the mechanism which may bring about such multidecadal variations in the teleconnection mechanism.

E. C. J. Oliver (✉)
Institute for Marine and Antarctic Studies, University of Tasmania, Hobart, Tasmania, Australia
e-mail: eric.oliver@utas.edu.au

Department of Oceanography, Dalhousie University, Halifax, Nova Scotia, Canada

1 Introduction

Wintertime surface air temperature (SAT) variability in Alaska occurs on many time scales. El Niño-Southern Oscillation (ENSO), the Pacific Decadal Oscillation (PDO), the polar jet stream and regional wind and radiative forcing patterns are all known to drive wintertime SAT variations in Alaska (Papineau 2001; Simpson et al. 2002). In winter, there exists a strong air temperature difference between areas over the sea and areas over land. Anomalous onshore and offshore winds, coupled with this strong cross-shore temperature gradient, lead to significant variations in wintertime SAT (Papineau 2001). In addition, the PDO is known to modulate sub-monthly SAT variability in Alaska by influencing the frequency of events along the polar jet stream (Papineau 2001).

The Madden–Julian Oscillation (MJO) is the dominant mode of atmospheric variability in the tropics on intraseasonal time scales (Zhang 2005). The MJO is expressed primarily through variations in zonal wind, precipitation and cloud cover with a period of 40–60 days and eastward propagation along the Equator. The MJO is strongest over the tropical Indo-Pacific although particularly strong MJOs can propagate around the entire Equator. Despite the tropical nature of the MJO, it is known to influence weather and climate in the extratropics, including the North Atlantic Oscillation (Cassou 2008; Lin et al. 2009), rainfall over the Pacific Northwest of the USA (Bond and Vecchi 2003) and the generation rate of tropical cyclones in all ocean basins (Hall et al. 2001; Maloney and Hartmann 2000a, b; Ho et al. 2006; Bessafi and Wheeler 2006). It has been established that the MJO is linked with intraseasonal variability of SAT at high latitudes in the Northern Hemisphere (Vecchi and Bond 2004; Lin and Brunet 2009). Wintertime SAT anomalies associated with the MJO are on the order of

Published online: 11 July 2014

5 °C in some regions. In particular, Alaska has been identified as an area with a strong connection between wintertime SAT and the MJO (Zhou et al. 2011).

The proposed connection mechanism between wintertime Alaska SAT and the MJO is based on a modulation of cross-shore temperature advection by the MJO (Zhou et al. 2011). The MJO excites a Rossby wave train in the tropical Indo-Pacific which propagates to the extratropical Northern Hemisphere. These Rossby waves have a detectable signal in the geopotential height of the 500-hPa surface and in sea level pressure, and therefore lead to anomalous geostrophic surface winds. As these Rossby waves pass over Alaska, the associated anomalous onshore and offshore winds lead to intraseasonal variations in wintertime temperature advection and thus SAT. These Rossby waves form the teleconnection mechanism by which the MJO, a tropical phenomenon, is able to influence Alaska air temperature, i.e., extratropical weather. It is important to note that these waves do not advect temperature anomalies from the tropics to the extratropics. Instead, they modulate the North Pacific wind field and influence Alaska air temperature through local temperature advection across the strong cross-shore temperature gradient.

We have undertaken an examination of the connection between the MJO and Alaska wintertime SAT on multidecadal time scales, in order to examine this connection over a much longer time period than has been done previously and to identify the presence or absence of any "climate shifts." This is enabled by both station records of Alaska SAT (at Fairbanks and Nome), which span the twentieth century, and a recent independent reconstruction of the MJO index over the 1905–2008 period (Oliver and Thompson 2012). In examining the MJO–SAT connection over the entire twentieth century, we identify significant multidecadal variability in its strength which is in turn related to variations in the magnitude of intraseasonal cross-shore temperature advection.

2 Data

Two indices of the MJO index were used in this study. First, daily values of the Wheeler and Hendon (2004) index, I^{WH}, were obtained from the Bureau of Meteorology, Australia, for the period of 1979 to 2010. The Wheeler and Hendon (2004) index consists of the first two principal component time series (with most of their energy between about 30 and 90 days) of tropical outgoing long-wave radiation and zonal wind at 250 and 850 hPa. Second, daily values of the historical reconstruction of the MJO index, I^{HR}, by Oliver and Thompson (2012), were obtained from http://passage.phys.ocean.dal.ca/~olivere/. The historical reconstruction was derived from a multivariate linear regression of I^{WH} onto surface pressure time series at selected locations from the 20th Century Reanalysis Project (Compo et al. 2011) over 1979–2008 and reconstructed back to 1905. Here, we define the "modern period" as being 1979–2008 and the "full record" as being 1905–2008. While our analysis of multidecadal variability will rely on I^{HR}, we have included I^{WH} in the analysis to provide a validation over the modern period.

The MJO index is often represented in "MJO phase space," whereby the second component of the index is plotted against the first component. Trajectories following the MJO index in time typically follow a counterclockwise path in phase space as an event propagates eastward around the globe. The radius and angle of a particular point in phase space represents the strength and phase of the MJO, respectively, and the angle can also be interpreted as the region over which the active convection associated with the MJO is situated. Phase space is usually divided into nine regions: a "weak MJO" region defined for amplitude less than one and eight regions (denoted "phase 1" through "phase 8") spaced equally around the remainder of phase space (Wheeler and Hendon 2004). The centre of MJO convection is over the Western Hemisphere and Africa during phases 8 and 1, the Indian Ocean during phases 2 and 3, the Maritime Continent during phases 4 and 5, and the Western Pacific during phases 6 and 7. One MJO phase corresponds to roughly 5–8 days. A traditional method of analysing the MJO-related behaviour of a particular variable is to calculate composites of that variable with each of the eight MJO phases.

Two time series of daily minimum SAT were obtained for Fairbanks and Nome (Alaska, USA) spanning over 100 years. Details on the temperature records, such as station location, exact time period covered and completeness, can be found in Table 1. The seasonal cycle was removed from each series by harmonic regression (the annual cycle and its first two harmonics) prior to analysis, and the residual is denoted T.

Daily fields of 2-m SAT, 10-m zonal and meridional winds, sea level pressure (SLP), and 500-hPa geopotential height were obtained from the 20th Century Reanalysis Project (20CR) for the period of 1905 to 2008 (Compo et al. 2011). The 20CR was carried out on a global grid with 2° horizontal resolution in latitude and longitude and assimilates only SLP and surface pressure observations, monthly sea surface temperatures, and sea ice distributions using a 58-member ensemble Kalman smoother. Note that the Fairbanks and Nome temperature data are independent from the 20CR data since the reanalysis did not assimilate air temperature records.

The PDO, a lower-frequency El Niño-type pattern in the Pacific Ocean, is characterised by the PDO index of Mantua et al. (1997). We obtained a time series of monthly PDO index values (1900–2013) from

Table 1 The long Alaska daily minimum surface air temperature (SAT) records

Location	Latitude	Longitude	Start	End	Percentage
Farbanks, AK, USA	64°50′ N	147°43′ W	1 August 1904	31 July 2010	99.4
Nome, AK, USA	64°30′ N	165°24′ W	1 August 1906	31 July 2010	99.6

The records were obtained from the Alaska Region Headquarters of the National Weather Service, USA (http://www.arh.noaa.gov/). The numbers in the final column indicate the percent completeness of the time series

http://jisao.washington.edu/pdo/PDO.latest. We then calculated an annual index of average wintertime (December–January–February) PDO values, indexed by the year corresponding to the January of each winter.

3 Results

In this section, we present the observed relationship between the MJO and Alaska SAT time series over the last century including its multidecadal variability (Section 3.1) followed by an illustration of the teleconnection mechanism (Section 3.2) and an interpretation in terms of variations in the teleconnection mechanism (Section 3.3).

3.1 Connection between Alaska SAT and the MJO in the twentieth century

We have quantified the relationship between SAT and the MJO by means of a linear regression onto the two components of the MJO:

$$T_t = \beta_0 + \beta_1 I_{1,t} + \beta_2 I_{2,t} + \epsilon_t, \tag{1}$$

where T_t is SAT at time t; $I_{1,t}$ and $I_{2,t}$ are the first and second components of the MJO index respectively; β_0, β_1 and β_2 are regression coefficients; and ϵ_t is a model error term. Estimates of the regression coefficients, $\hat{\beta}_0$, $\hat{\beta}_1$ and $\hat{\beta}_2$, are calculated by least squares. Maps of $\hat{\beta}_1$ and $\hat{\beta}_2$ can be interpreted as "response patterns" of SAT to I_1 and I_2, respectively. The regression approach provides a linear alternative to the traditional compositing technique (e.g., Wheeler and Hendon (2004); Vecchi and Bond (2004)) while providing similar results in a more computationally efficient manner (Oliver 2011). In contrast, the benefits of composite analysis is that small variations (e.g., less than 1 standard deviation) are ignored and the focus is thus on less noisy signals.

The regression provides an equivalent of the traditional 8-phase composite plots, referred to as the "MJO response," which is simply an idealised representation of the connection between a given variable and the MJO based on the regression model. The "MJO response" of T_t is given by

$$T_t^{\mathrm{MJO}} = \hat{\beta}_1(a\cos\phi) + \hat{\beta}_2(a\sin\phi). \tag{2}$$

where we have removed the mean (β_0) and the error term (ϵ_t) from Eq. 1, replaced the regression coefficients (β_1 and β_2) with their least-squares estimates, and replaced the MJO index with an idealised sinusoidal variation of the form $[I_{1,t}, I_{2,t}] = [a\cos\phi, a\sin\phi]$, where $\phi = -7\pi/8, -5\pi/8 \ldots 7\pi/8$ (corresponding to the MJO phases 1,2...8) and a is the MJO amplitude. We selected an amplitude of $a = 1.5$ for the following analysis in order to examine the response due to a moderate/strong MJO cycle. The "MJO response" is similar to composite averages according to MJO phase except that composites are an average (which may include an estimate of variance for calculation of statistical significance), while the "MJO response" involves least squares fitting.

We can also interpret the MJO response in terms of the magnitude of the response and the MJO phase at which this magnitude peaks. This can be calculated by transforming the regression coefficients as follows. The magnitude of the MJO response is given by

$$A = a\sqrt{\hat{\beta}_1^2 + \hat{\beta}_2^2} \tag{3}$$

and the phase is given by

$$\theta = \arctan(\hat{\beta}_2/\hat{\beta}_1). \tag{4}$$

We can use maps of A and θ to examine the strength and timing of the response of T_t to the MJO. See Zhou et al. (2011) for another example of this in the MJO literature.

The MJO response of wintertime (defined as December–January–February, or DJF) T at Fairbanks and Nome, due to an ideal MJO cycle of amplitude 1.5, indicated a strong relationship (Fig. 1, thick lines). The maximum T response, for I^{WH}, occurred in phase 1 (8) with magnitude 4.5 °C (4 °C) at Fairbanks (Nome). Due to the linear nature of the technique (see Eq. 2), the minimum response was of exactly opposite magnitude four phases later. Similar results were found for wintertime maximum temperature (this is not surprising since, after removing the seasonal cycle, wintertime maximum SAT and minimum SAT had a correlation coefficient of 0.90 and 0.91 at Fairbanks and Nome, respectively).

The response of wintertime T to I^{HR} was broadly consistent with the response to I^{WH} (Fig. 1, compare thin and thick lines) validating the use of I^{HR} for analysing the MJO–Alaska SAT connection. The maximum response of

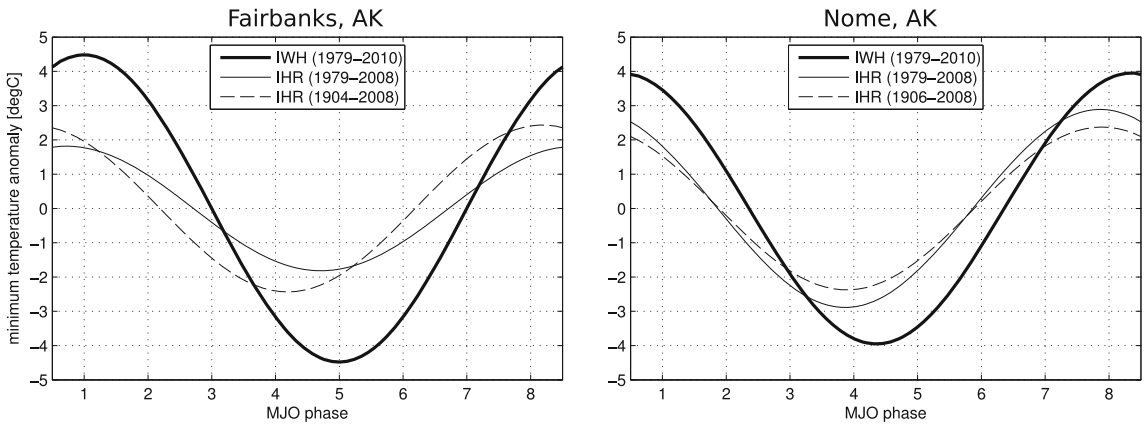

Fig. 1 Connection between the MJO and Alaska station SAT. The MJO response of wintertime SAT at (**a**) Fairbanks and Nome due to an MJO cycle of amplitude 1.5 is shown for I^{WH} (*thick solid line*, calculated over the modern period 1979–2010), (**b**) I^{HR} (*thin solid line*, calculated over the modern period 1979–2008), and (**c**) I^{HR} (*dashed line*, calculated over the full record 1904(1906)–2008 for Fairbanks (Nome))

T, for I^{HR} calculated over the modern period, occurs at nearly the same phase (within an error of ∼0.5 MJO phases) although the magnitude is reduced by approximately half: ∼2 °C (2.5 °C) for Fairbanks (Nome). We note that the MJO response exists over both the modern period and the full record, indicating that the connection between the MJO and Alaska wintertime SAT has persisted over at least a century.

In order to examine any changes in the connection between wintertime T at Fairbanks and Nome over centennial time scales, we calculated the MJO response in moving 15-year blocks over the full record (Fig. 2). We tested moving 10- and 20-year blocks without a significant difference in the results; moving blocks of length less than 10 years result in poor statistical significance due to small sample sizes. The results over the modern period were consistent between the I^{HR} and I^{WH} indices (compare Fig. 2a, b for Fairbanks and Fig. 2c, d for Nome). Over the full record, certain time periods showed a strong response to the MJO (such as 1946–1966 for both Nome and Fairbanks or 1910–1919 for Fairbanks), while other periods showed a weaker response (such as 1970–2000) or no response at all (1920–1945 for Fairbanks, 1910–1945 for Nome). For periods when there existed a response, negative temperature anomalies tended to occur during MJO phases 1–6 and positive temperature anomalies during phases 1–2 and 6–8 with a magnitude of ±4–6 °C which is consistent with Vecchi and Bond (2004). Note that the timing of the response varies slightly over the full record.

From these results discussed above, we have defined four distinct time periods: 1910–1919 (P1; moderate response),

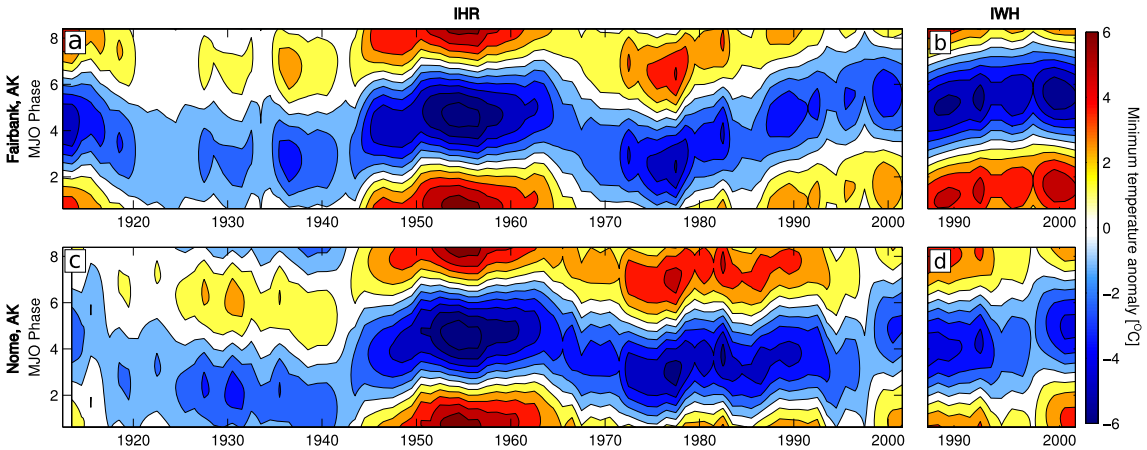

Fig. 2 Connection between MJO and Alaska station SAT over the twentieth century. The MJO response of wintertime SAT, calculated over running 15-year blocks, at **a**, **b** Fairbanks and **c**, **d** Nome due to an MJO cycle of amplitude 1.5 is shown for **a**, **c** I^{HR} and **b**, **d** I^{WH}. Note that all panels share the same colour scale

1920–1945 (P2; weak response), 1946–1966 (P3; strong response) and 1970–2000 (P4; moderate response). These time periods are defined qualitatively from a visual analysis of Fig. 2a, c and Fig. 3b. The p value of the regression shown in this figure for the strong and moderate responses during P1 (Fairbanks only), P3 and P4 is generally less than 0.05 and for the weak responses during P1 (Nome only) and P2 is generally greater than 0.05.

The PDO is known to play a role in Alaska temperature variations on multidecadal time scales (Papineau 2001). The response amplitude of MJO-related SAT DJF T to the MJO shows significant multidecadal variability, and there is some clear covariability with the PDO index (Fig. 3). The correlation coefficient is −0.64 (Fairbanks) and −0.56 (Nome), with a p value less than 0.01. Notably, periods of strong MJO response in SAT tend to occur during negative (1946–1966) or neutral (1910–1919) PDO periods, and weak MJO response in SAT tends to occur during positive (1920–1945) PDO periods. This relationship does not explain all of the variability in the MJO response as there are periods of negative PDO without a strong MJO response in SAT (late 1960s and early 1970s) and periods of positive PDO without a weak MJO response in SAT (1980s and early 1990s).

The amplitude of the MJO response of wintertime T to I^{HR} over the entire Alaska region was calculated over the four time periods from fields of 20CR SAT (Fig. 4; phase of peak response not shown). The magnitudes of the response of 20CR SAT over Alaska were generally consistent with the independent observations at Fairbanks and Nome: (P1) 1910–1919 (moderate response; ±1.5 °C peaking in phases 7–8 and 1–2), (P2) 1920–1945 (weak response; ±1 °C peaking in phases 8 and 1), (P3) 1946–1966 (strong response; ±3 °C peaking in phases 8 and 1), and (P4) 1970–2000 (moderate response; ±2 °C peaking in phases 6–8 and 1). Note that the SAT response in P4 (Fig. 4d) is weaker than that calculated by Vecchi and Bond (2004) (their Fig. 2). This may be due to a difference between the response of wintertime Alaska SAT to the two MJO indices (compare left and right panels in Fig. 2) as well as the 20CR possibly not able to capture the full range of SAT variability present in the station observations (which are not assimilated by 20CR).

It is important to note that these changes were not due to multidecadal changes in the strength of the MJO since the regression method used to calculate these MJO response patterns was insensitive to variability in MJO amplitude: if the relationship between MJO and T remained the same, then the regression coefficients would be constant in time regardless of variations in MJO amplitude. In technical terms, the MJO response patterns shown in Figs. 2 and 4 are the response of T to an MJO event of amplitude 1.5 based on the temporally local regression coefficients, regardless of the local MJO amplitude. This is different from a composite approach for which multidecadal variations in MJO amplitude will be reflected by multidecadal variations in the composite average. Using the present technique, if the connection mechanism remains stable, multidecadal variations in MJO amplitude result in constant regression coefficients. Therefore, it is suggested that the observed multidecadal variability is due to variations in the mechanism and that links MJO and Alaska wintertime SAT variability.

3.2 The teleconnection mechanism

The teleconnection mechanism between the MJO and Alaska SAT consists of a train of Rossby waves originating in the tropics, where they are excited by the MJO, and which propagate into the extratropics. This Rossby wave train is detectable in dynamic variables including SLP, 500-hPa geopotential height and wind speed (e.g., Zhou et al. (2011)). The Rossby waves are clearly visible in the MJO reponse of 500-hPa geopotential height (Fig. 5). Following

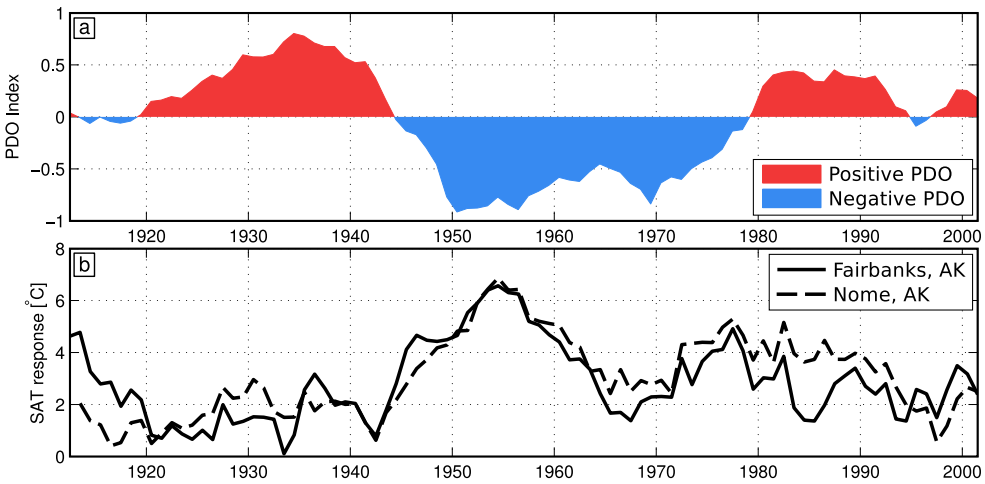

Fig. 3 Comparison of MJO-related and Alaska station SAT variations and the Pacific Decadal Oscillation (*PDO*). The PDO Index (DJF-only values, with a 15-year running average) is shown in panel **a** and the amplitude of the MJO response of wintertime SAT due to an MJO cycle of amplitude 1.5, calculated over running 15-year blocks, is shown in panel **b** for Fairbanks (*solid line*) and Nome (*dashed line*)

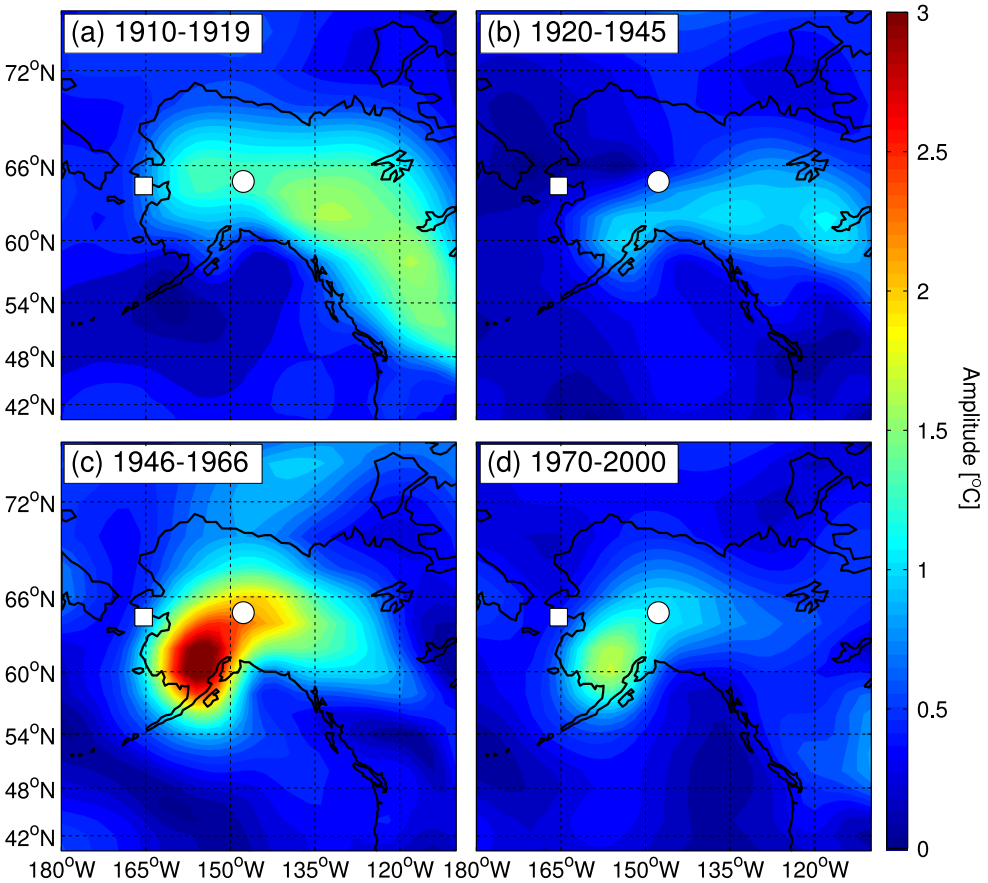

Fig. 4 Connection between MJO and Alaska-wide SAT in the twentieth century. The magnitude of the MJO response of wintertime SAT due to an MJO cycle of amplitude 1.5 is shown for four time periods: **a** 1910–1919, **b** 1920–1945, **c** 1946–1966 and **d** 1970–2000. The *circle* and *square* indicate the location of the Fairbanks and Nome stations, respectively

a particular wave in this train, indicated by the grey dot in Fig. 5, we can see that it propagates from subtropical East Asia (phase 1), across the North Pacific Ocean where it increases in magnitude just southwest of Alaska (phases 2–5), and subsequently partially dissipates and then continues propagating over northern North America (phases 6–8). During phase 8, we can see another Rossby wave entering the domain from the tropical southwest.

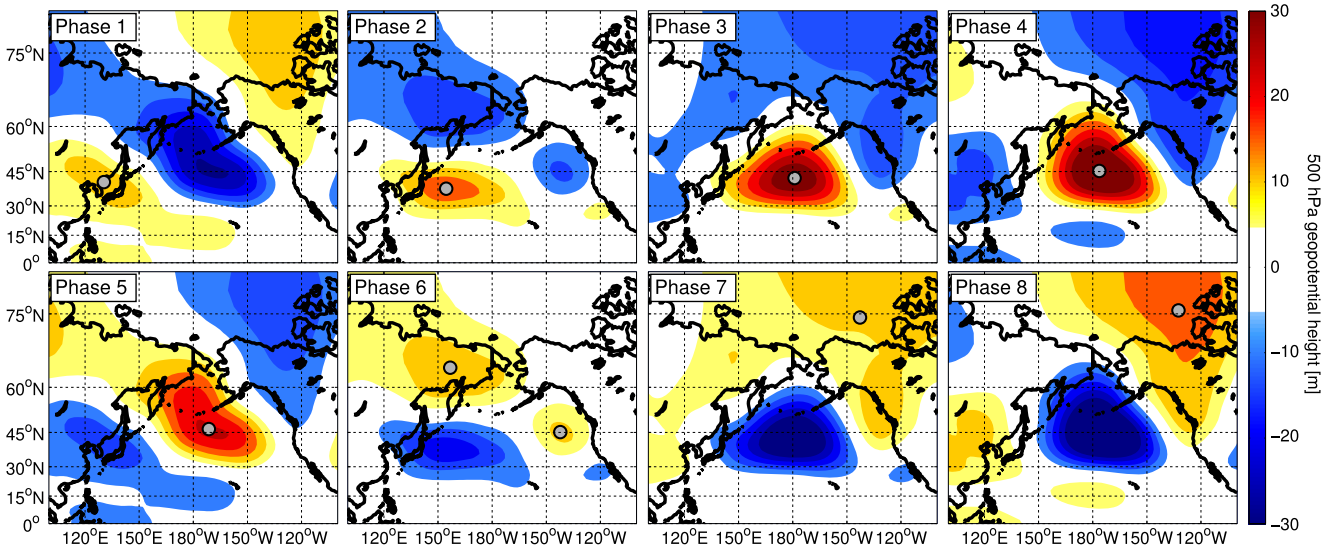

Fig. 5 The Rossby wave train driven by the MJO. The eight panels indicate the MJO response of 500-hPa geopotential height in each of the eight MJO phases (for an MJO of amplitude 1.5). The *grey dot* follows a single wave in the wave train as it propagates over Alaska

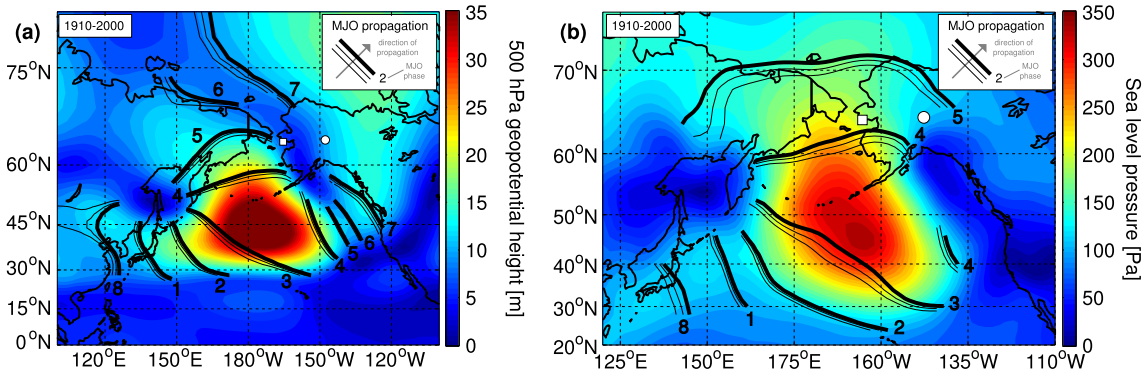

Fig. 6 The teleconnection pattern linking the MJO and Alaska SAT over the twentieth century. The MJO response of wintertime **a** 500-hPa geopotential height and **b** sea level pressure due to an MJO cycle of amplitude 1.5 is shown, calculated over 1910–2000. The *coloured contours* indicate the amplitude of the response (Eq. 3). The labelled *solid lines* indicate the integer MJO phase at which maximum response occurs at each point in space (Eq. 4; phase lines are not plotted for a response amplitude less than **a** 8 m or **b** 35 Pa). *Thin lines* demonstrate propagation direction of the response as the MJO moves through a cycle by indicating phases just prior to an integer MJO phase (e.g., a *solid line* indicates phase 1 while the *two thin lines* indicate phases 0.925 and 0.85). The *circle* and *square* indicate the location of Fairbanks and Nome, respectively

The MJO response of 500-hPa geopotential height (Fig. 5) can be reexpressed, following Eqs. 3 and 4, in terms of amplitude and phase (Fig. 6a) instead of the eight-panel phase plots. In this figure, the amplitude of the responseof 500-hPa geopotential height to the MJO is shown by the coloured contours, and the phase at which maximum response occurs at each point in space is shown by the labelled contours. It is clear from this figure that the MJO response of 500-hPa geopotential height reaches its peak (over 35 m) over the North Pacific during phases 3–4 and that the direction of propagation is from tropical East Asia to northern North America.

The MJO response of wintertime SLP was similar to that of 500-hPa geopotential height (Fig. 6b). The MJO modulates a region SLP southwest of Alaska of up to ±350 Pa with clear propagation from East Asia towards North America. This SLP anomaly caused anomalous poleward, or onshore, meridional surface winds over southern Alaska when it is positive during MJO phases 3–5 and equatorward, or offshore, meridional surface winds when the SLP anomaly is negative during the opposite MJO phases (7–8 and 1). These wind anomalies, coupled with the strong cross-shore SAT gradient (SAT is lower over land than over ocean), led to cooling from offshore wind anomalies during phases 3–5 and warming from onshore wind anomalies during phases 7–8 and 1. Therefore, this led to a minimum (maximum) temperature anomaly at the end of the cooling (warming) period, i.e., approximately in phase 5 (1). This was consistent with the MJO response of Alaska wintertime SAT (Section 3.1) and with the Rossby wave teleconnection pattern reported by Zhou et al. (2011).

3.3 Multidecadal variability of the teleconnection mechanism

The multidecadal changes in the MJO response of the Alaska SAT connection can be explained by changes in the teleconnection pattern presented in Section 3.2. The amplitude of the MJO response of wintertime SLP to I^{HR} was calculated over the four time periods identified in Section 3.1 (Fig. 7). It is clear that the SLP response was strong in P3 (1945–1965; Fig. 7c), of moderate strength in P1 and P4 (1910–1919 and 1970–2000; panels a and d of Fig. 7, respectively), and weak or nonexistent in P2 (1920–1945; Fig. 7b). These results were consistent with the multidecadal variation in the MJO–Alaska SAT connection (compare with Fig. 4). First, a strong MJO–SLP connection was apparent during 1946–1966 when the MJO–SAT connection was also strong. Second, during 1910–1919 and 1970–2000, the MJO–SLP connection was of moderate strength and the SLP anomaly was weaker and/or shifted spatially, reducing the efficacy of SAT modulation by temperature advection. Finally, during 1920–1945, the MJO–SLP connection has nearly disappeared and the weak wind anomalies associated with it would not strongly advect temperature across the Alaskan coastline.

As further evidence of this mechanism, we have calculated the multidecadal variation of MJO-related temperature advection. Temperature advection, as a rate of change of temperature (°C per unit time), is given by

$$\Delta_{\mathrm{adv}} = -u \cdot \nabla \overline{T}, \tag{5}$$

where u is a vector field of surface winds and $\nabla \overline{T}$ is the horizontal gradient of the mean SAT field. As noted

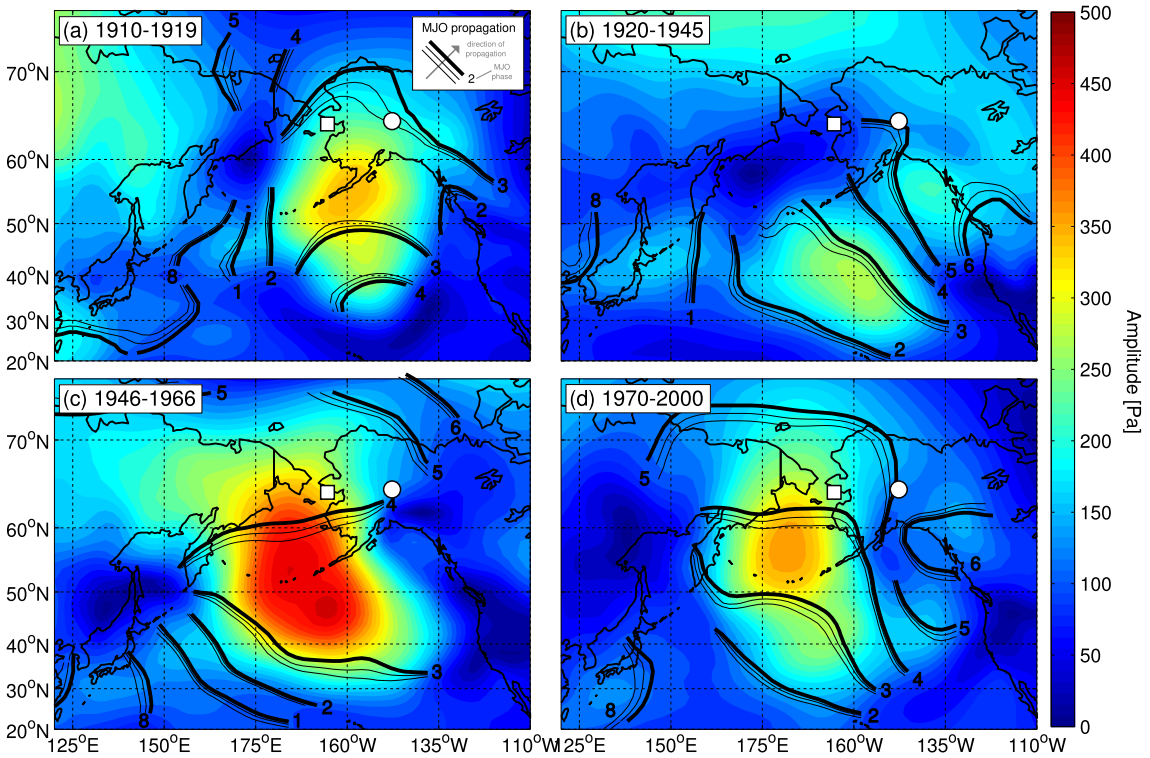

Fig. 7 Changes in the teleconnection pattern linking the MJO and Alaska SAT over the twentieth century. The magnitude of the MJO response of wintertime sea level pressure due to an MJO cycle of amplitude 1.5 is shown for four time periods: **a** 1910–1919, **b** 1920–1945, **c** 1946–1966 and **d** 1970–2000. The *solid lines* indicate the MJO phase of maximum response (not plotted for an amplitude less than 35 Pa). The *circle* and *square* indicate the location of Fairbanks and Nome, respectively

above, $\nabla\overline{T}$ is large near the coast and so a cross-shore u will lead to temperature advection. We calculated a time series of Δ_{adv} given the surface wind time series and the mean SAT field for each of the four periods defined above. The MJO response of wintertime Δ_{adv}, over the four time periods identified in Section 3.1, showed multidecadal variations that were broadly consistent with the variations in the MJO response of Alaska SAT (Fig. 8). In particular, the MJO response of Δ_{adv} was strongest over 1945–1965 (exceeding 2 °C/day in some regions), corresponding to the period of maximum SAT response, and weaker during the other three periods (<1.5 °C/day). Interpolated to the location of Fairbanks, Δ_{adv} was largest during P3, smallest during P2 and of moderate value during P1 and P4; interpolated to the the location of Nome, Δ_{adv} was largest during P3, smallest during P1 and slightly larger during P2 and P4—broadly consistent with the pattern shown in Fig. 2. A typical value for temperature advection at these location is $\sim \pm 0.5$ °C/day which, if we assume that the MJO actively advects temperature in the region over two MJO phases and that each MJO phase lasts approximately 5 days, leads to a temperature variation of $\sim \pm 5$ °C, consistent with Fig. 2.

The PDO has a strong influence on the cross-shore SAT gradient between Alaska and the North Pacific Ocean (Fig. 9). The mean wintertime SAT pattern, over 1905–2008, indicated a strong cross-shore SAT gradient with temperatures as low as −10 to −20 °C over central Alaska and as high as 10 to 20 °C over the North Pacific Ocean (Fig. 9a). Composites of wintertime SAT anomalies with positive and negative phases of the PDO indicated a modulation of this general pattern by the PDO. Positive and negative phases of the PDO were defined by PDO values greater (less) than +0.5 (−0.5) standard deviations from the mean. A positive PDO led to positive SAT anomalies over Alaska and negative SAT anomalies over the North Pacific Ocean, while a negative PDO led to the opposite pattern, consistent with Papineau (2001) (anomalies of approximately 1 °C magnitude; Fig. 9b,c). Therefore, a negative PDO acted to increase the cross-shore SAT gradient, and thus the cross-shore temperature advection (see Eq. 5), while a positive PDO acted to reduce the cross-shore SAT gradient and temperature advection. This mechanism may explain the multidecadal variability in the MJO connection to wintertime Alaska SAT and the anti-correlation

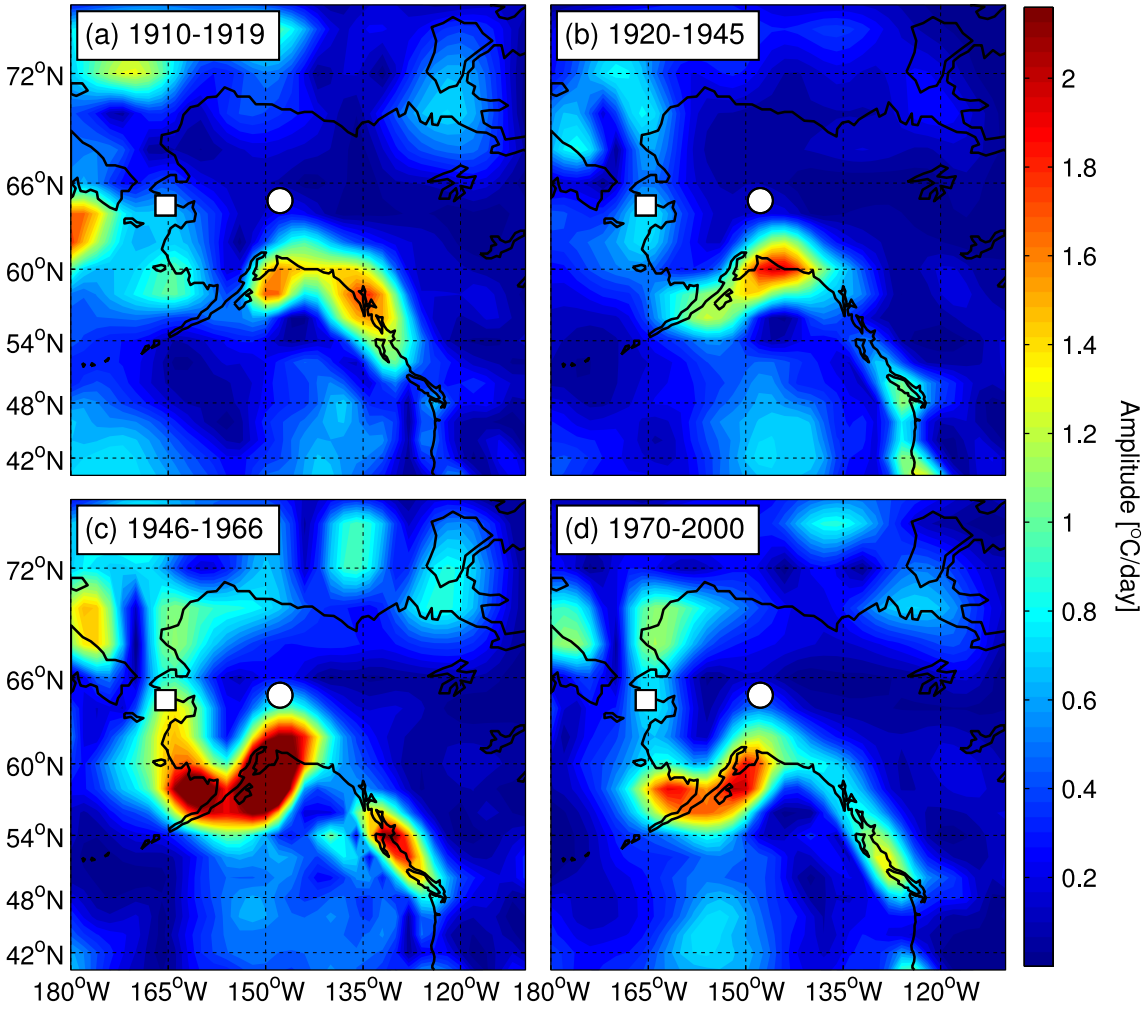

Fig. 8 Changes in temperature advection around Alaska due to the MJO over the twentieth century. The magnitude of the MJO response of wintertime temperature advection due to an MJO cycle of amplitude 1.5 is shown for four time periods: **a** 1910–1919, **b** 1920–1945, **c** 1946–1966 and **d** 1970–2000. The *circle* and *square* indicate the location of Fairbanks and Nome, respectively

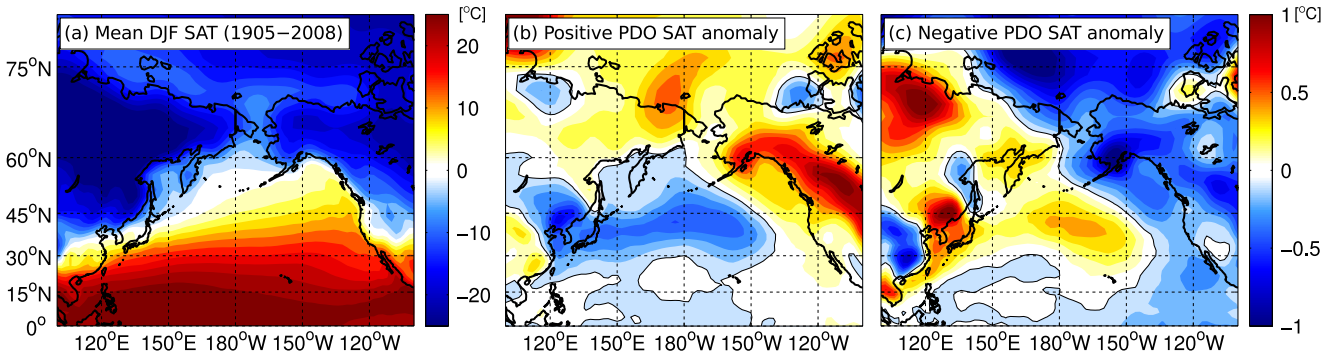

Fig. 9 Mean wintertime SAT pattern and the influence of the PDO. The mean wintertime SAT is shown **a** along with composites of SAT anomalies for positive **b** and negative **c** phases of the PDO. Positive and negative phases of the PDO were defined by PDO values greater (less) than +0.5 (−0.5) standard deviations from the mean

between the magnitude of this connection and the PDO index.

4 Summary and discussion

In this study, we have demonstrated that the connection between the Madden–Julian Oscillation and wintertime Alaska surface air temperature is subject to multidecadal variability over the twentieth century. We first showed that the response of wintertime SAT measured at Fairbanks and Nome to the MJO varied between nearly zero during certain periods to up to a ±6 °C modulation. From this, we identified four time periods each with a distinct MJO response level: 1910–1919 (P1; moderate response), 1920–1945 (P2; weak response), 1946–1966 (P3; strong response) and 1970–2000 (P4; moderate response). Furthermore, we showed that the MJO response of sea level SLP, and thus cross-shore wind and temperature advection, forms the teleconnection mechanism linking the MJO to Alaska SAT and that this mechanism has undergone the same multidecadal variations over the twentiethcentury.

The multidecadal variations in the MJO response of Alaska SAT show moderate links to the PDO. However, while the correlation of MJO-related variability is significant and some covariability is obvious from direct comparison of the time series, the PDO does not explain all the variations in the MJO response. Notably, the strong climate shift that occurred in the North Pacific in the late 1970s, as evidenced by the change in PDO index value (Fig. 3), is not reflected in the MJO response of Alaska SAT. While the MJO response of Alaska SAT undergoes a dramatic positive shift in the mid-1940s, coinciding with the onset of a strong negative PDO, it undergoes a negative shift in the late 1950s and 1960s, at least 10 years before the climate shift in the 1970s . Nevertheless, the links between the MJO response of Alaska SAT and the PDO, particularly through the modulation of the cross-shore temperature gradient by the PDO, lead to the conclusion that the role of the MJO and the PDO on intraseasonal SAT variability in this region are not completely independent.

A Rossby wave train originating in the tropics, forced by the MJO, and propagating over Alaska leading to cross-shore temperature advection forms the dynamics of the teleconnection mechanism (Zhou et al. 2011). The MJO index has not undergone significant multidecadal variations over the twentieth century (Oliver and Thompson 2012), and so it is suggested that the variations in the MJO–SAT connection identified here are due to multidecadal variability in the teleconnection mechanism itself. The path and/or magnitude of the poleward-propagating Rossby waves could be modified by changes to the background state (for example, by the PDO), as is the case for stationary Rossby waves (e.g., Hoskins and Karoly (1981); Karoly (1983); Hoskins and Ambrizzi (1993)). An examination of the changes to Rossby wave propagation due to changes in the background state would be required to address this question, which is beyond the scope of the present work.

Acknowledgments The authors would like to acknowledge the various anonymous reviewers for helping to strengthen the manuscript as well as Prof. Keith Thompson for helpful discussions.

References

Bessafi M, Wheeler M (2006) Modulation of South Indian Ocean tropical cyclones by the Madden–Julian oscillation and convectively coupled equatorial waves. Mon Weather Rev 134:638–656

Bond N, Vecchi G (2003) The influence of the Madden–Julian Oscillation on precipitation in Oregon and Washington. Weather Forecast 18(4):600–613

Cassou C (2008) Intraseasonal interaction between the Madden-Julian Oscillation and the North Atlantic Oscillation. Nat 455(7212):523

Compo G, Whitaker J, Sardeshmukh P, Matsui N, Allan R, Yin X, Gleason B, Vose R, Rutledge G, Bessemoulin P et al (2011) The twentieth century reanalysis project. Q J R Meteorol Soc 137(654):1–28

Hall J, Matthews A, Karoly D (2001) The modulation of tropical cyclone activity in the Australian region by the Madden–Julian Oscillation. Mon Weather Rev 129(12):2970–2982

Ho C, Kim J, Jeong J, Kim H, Chen D (2006) Variation of tropical cyclone activity in the South Indian Ocean: El Niño–Southern Oscillation and Madden-Julian Oscillation effects. J Geophys Res 111(D22):D22,101

Hoskins BJ, Ambrizzi T (1993) Rossby wave propagation on a realistic longitudinally varying flow. J Atmos Sci 50(12):1661–1671

Hoskins BJ, Karoly DJ (1981) The steady linear response of a spherical atmosphere to thermal and orographic forcing. J Atmos Sci 38(6):1179–1196

Karoly DJ (1983) Rossby wave propagation in a barotropic atmosphere. Dyn Atmos Oceans 7(2):111–125

Lin H, Brunet G (2009) The influence of the Madden–Julian Oscillation on Canadian wintertime surface air temperature. Mon Weather Rev 137:2250–2262

Lin H, Brunet G, Derome J (2009) An observed connection between the North Atlantic oscillation and the Madden–Julian oscillation. J Clim 22:364–380

Maloney E, Hartmann D (2000a) Modulation of Eastern North Pacific hurricanes by the Madden–Julian Oscillation. J Clim 13(9):1451–1460

Maloney E, Hartmann D (2000b) Modulation of hurricane activity in the gulf of Mexico by the Madden-Julian Oscillation. Sci 287(5460):2002

Mantua NJ, Hare SR, Zhang Y, Wallace JM, Francis RC (1997) A pacific interdecadal climate oscillation with impacts on salmon production. Bull Am Meteorol Soc 78(6):1069–1079

Oliver E (2011) Ph.D. Thesis: Local and remote forcing of the ocean by the Madden-Julian Oscillation and its predictability, Dalhousie University, Halifax, Canada

Oliver E, Thompson K (2012) A reconstruction of Madden-Julian Oscillation variability from 1905 to 2008. J Clim 25(6):1996–2019

Papineau JM (2001) Wintertime temperature anomalies in Alaska correlated with ENSO and PDO. Int J Climatol 21(13):1577–1592

Simpson JJ, Hufford GL, Fleming MD, Berg JS, Ashton JB (2002) Long-term climate patterns in Alaskan surface temperature and precipitation and their biological consequences. IEEE Trans Geosci Remote Sens 40(5):1164–1184

Vecchi G, Bond N (2004) The Madden-Julian Oscillation (MJO) and northern high latitude wintertime surface air temperatures. Geophys Res Lett:31

Wheeler M, Hendon H (2004) An all-season real-time multivariate MJO index: development of an index for monitoring and prediction. Mon Weather Rev 132(8):1917–1932

Zhang C (2005) Madden-Julian Oscillation. Rev Geophys 43:1–36

Zhou Y, Thompson K, Lu Y (2011) Mapping and understanding the relationship between northern hemisphere winter surface temperature and the Madden Julian Oscillation. Mon Weather Rev 139(8):2439–2445